Stars and their variability observed from space
C. Neiner, W. W. Weiss, D. Baade, R. E. Griffin, C. C. Lovekin, A. F. J. Moffat (eds)

DISKS AROUND BE STARS AND COMPLEX RADIATION EFFECTS

N. D. Kee[1]

Abstract. Observations of classical Be stars show significant variability in the signatures arising from their circumstellar disks on relatively short (month to year) times-cales. Indeed, it is even inferred that these stars are able to construct and fully destroy their disks in those short times. Given the high luminosity of the massive stars at the centre of the systems, interpreting and understanding the observations requires detailed modelling of the often quite complex interplay of stellar irradiation with disk material. This paper discusses recent efforts in that modelling, including the treatment of radiative acceleration of disk material, the thermal structure of the disk, and the role that these effects play in the observed variability of classical Be stars.

Keywords: Processes: hydrodynamics, radiative transfer, stars: circumstellar matter, emission-line, Be, winds, outflows

1 Introduction

In addition to their intrinsic stellar variability, classical Be stars also drive significant variations in their near-star environments by sculpting, constructing, and destroying their circumstellar disks on time-scales of a month to a year (Rivinius et al. 2013). It is this variability of the "stellar sphere of influence" that is addressed here. Even within this category of variations in the circumstellar environment, however, a wide variety of signatures are observed or expected from theory, and include photometric, spectroscopic and polarimetric variability, as well as combinations thereof. Therefore, in order to prioritize a detailed discussion over a broad overview, we are emphasising two active areas of study: (1) spectro-polarimetric diagnostics of the disk temperature and density structure, and (2) UV radiation-driven disk destruction.

For both of these sub-topics, the irradiation from the star itself is a key factor in driving the variability and forming the observable signatures. The following discussion is therefore centred around radiation transfer and radiation hydrodynamics. The primary focus is on the role of the stellar illumination in irradiating and heating the disk to generate the observed spectropolarimetric signatures. In Section 3, it is the role of UV irradiation to impart momentum to the disk material, and the attendant disk destruction mechanism that is emphasised.

2 Diagnosing disk density, size, and temperature with spectropolarimetry

To set up a discussion of the predicted spectropolarimetric signatures and how they depend on disk structure, it is first important to highlight the overall morphology of such signatures as observed in classical Be stars. For the purposes of this discussion, we focus on the region of the Balmer and Paschen jumps, specifically from about $\lambda\,3000$–$9000\,\text{Å}$. As shown in Fig. 1 (adapted from Quirrenbach et al. 1997, their Figure 6), the characteristic polarization signature in this region is at a level of a few percent, with a saw-tooth pattern imprinted onto it by the unpolarized hydrogen bound-free opacity.

By comparing these observations to theoretical predictions of the spectropolaremetric signature, as shown in Fig. 2 (adapted from Halonen & Jones 2013, their Figures 1, 4, 5, and 7), we see that theoretical models reproduce that general morphology of a saw-toothed pattern, and also the few-percent level of polarization. Additionally, taking each panel of Figure 2 individually, we also see that varying the disk size, density and thermal structure all introduce marked differences into the spectropolarimetric signature, much larger than the errors in the observed polarization signatures shown in Fig. 1. Conversely, from a comparison of all four panels of Fig. 2, we also see that there are degeneracies between the impact these different physical variations have on the spectropolarimetric signatures. The long history of studies of classical Be stars has revealed a plethora of

[1] Institute of Astronomy, KU Leuven, Celestijnenlaan 200D, B-3001 Leuven, Belgium
e-mail: dylan.kee@kuleuven.be

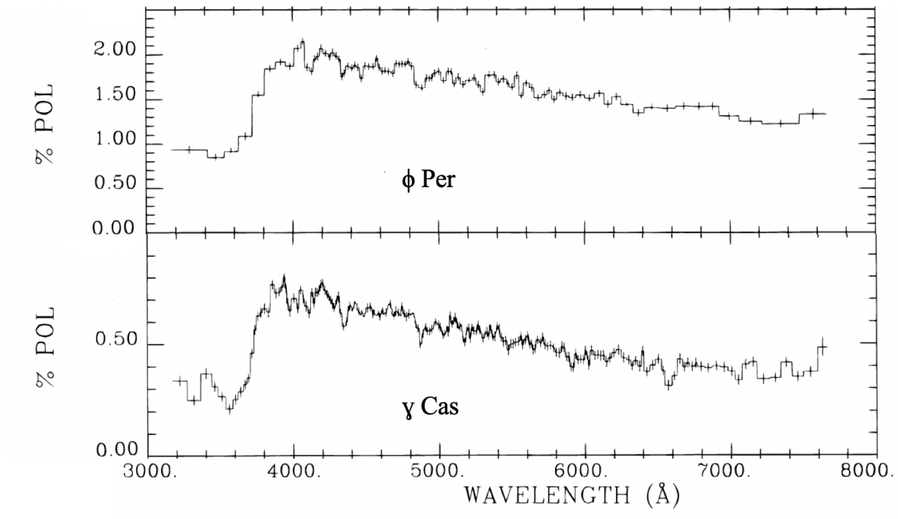

Fig. 1. Spectropolarimetric observations of two classical Be stars, showing the percentage of polarization as a function of wavelength across the Balmer jump. Adapted from Quirrenbach et al. (1997).

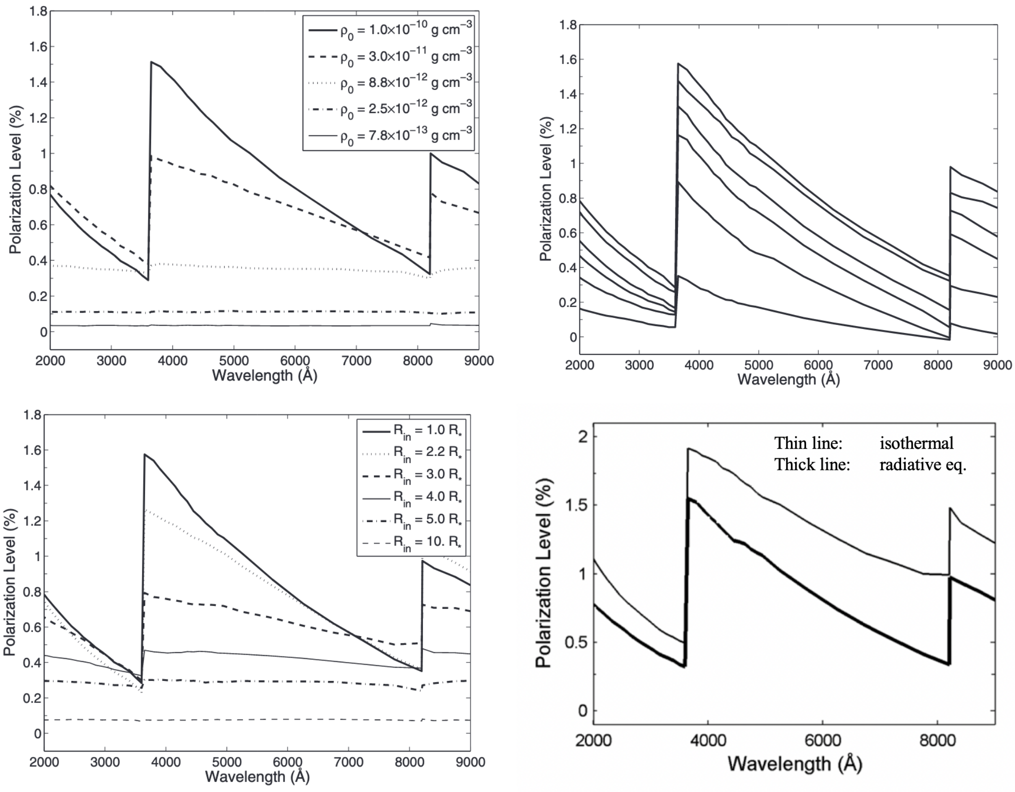

Fig. 2. Effects on the predicted polarization degree across the Balmer and Paschen jumps for a B2 star arising from varying **Top Left:** disk density (increasing density from bottom to top), **Top Right:** size of the disk (outer radius increasing from bottom to top), **Bottom Left:** the size of the gap between the disk inner edge and the star (increasing from top to bottom), and **Bottom Right:** the thermal structure of the disk, specifically here whether the disk is in radiative equilibrium or is isothermal at 0.6 times the stellar effective temperature. Adapted from Halonen & Jones (2013).

additional information derived from spectroscopy and photometry of classical Be stars (see, e.g. Rivinius et al. 2013, for a review); however, that synergizes well with the information available through spectopolarimetry, and simultaneous modelling of the spectropolarimetric signature alongside other observational diagnostics may lift this degeneracy

In addition to spectropolarimetric observations of fixed axisymmetric disks, time-resolved observations of the signatures from asymmetric disks can also assist in interpreting the morphology of classical Be stars. As shown by Marr et al. (2018), even simplified models for warping and over/under-densities in the disk generate noticeable variations in both the overall level of polarization and the strength of the Balmer/Paschen jumps. Figure 3 (adapted from Marr et al. 2018, their Figure 2) emphasises this point by showing the phased variation in both overall polarization (measured in the V band as an average of the polarization at $\lambda\,5250$ and $5750\,\text{Å}$) and the change in polarization over the Balmer jump for disks with a $10\times$ over-density in an azimuthal segment of 45, 90, 180 or 270 degrees, as labelled in the Figure. Both these signatures can clearly be seen to vary considerably with the phased viewing position of the disk, emphasising the additional information embedded in such time-resolved signatures.

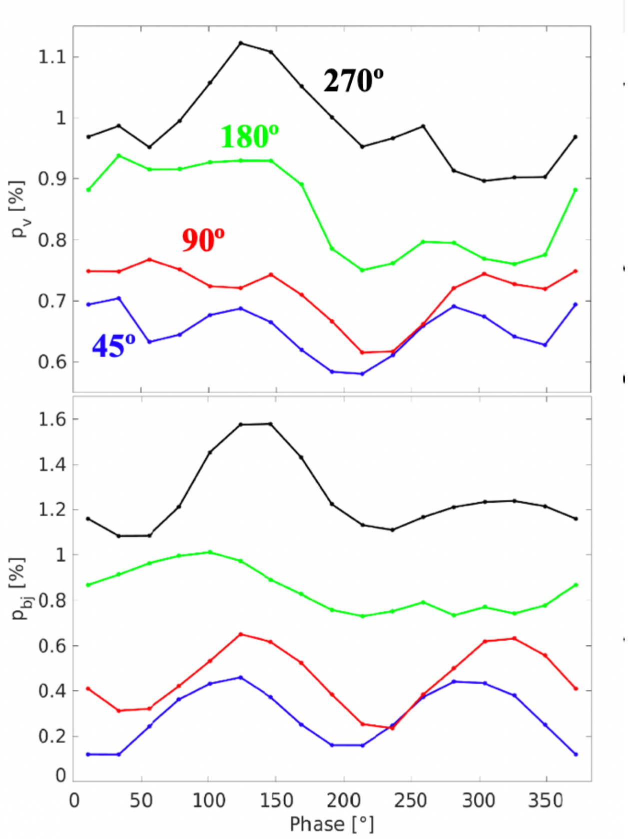

Fig. 3. Phase dependence of the polarization degree (**Top**, averaged from $\lambda\,5250$ and $5750\,\text{Å}$) and change in polarization across the Balmer jump (**Bottom**, difference between $\lambda\,3800$ and $3600\,\text{Å}$) for a simple model of an over-dense wedge in a disk of angular extent 45°, 90°, 180°, or 270° in azimuth, as labelled in the Figure. Adapted from Marr et al. (2018).

3 Disk destruction by UV line-driven disk ablation

We now turn our attention to studies of disk destruction, attempting to understand the rapid times – a month to a year – in which classical Be stars are able to lose their disks. Again motivated by the brightness of the central star, we emphasise the role that stellar irradiation may play in this process. This section actually parallels the discussion of UV line-driven disk ablation introduced by Kee et al. (2016).

The central concept here is that the standard model of UV line-driven winds as introduced by Castor et al. (1975) allows for the computation of acceleration from a local velocity gradient. When one accounts for the non-radial photons near the stellar surface that arise because of the finite size of the star, such velocity gradients can arise from the projection of non-radial motions, e.g. Keplerian rotation of the disk, onto the flight direction of the photon, thereby allowing photons from the star to drive acceleration of disk material. As shown by Fig. 4

(adapted from Kee et al. 2016, their Figures 5 and 6), this results in the acceleration of disk material in thin sheets along the surfaces of the disk to high velocities comparable with the speed of the wind.

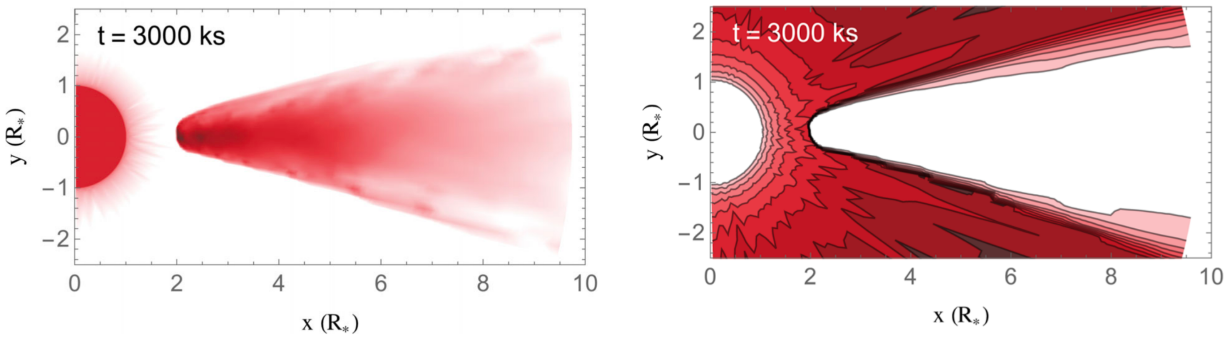

Fig. 4. Morphology of disk ablation shown in **Left:** density and **Right:** radial velocity, emphasising that the thin ablation layer is at disk-like densities but wind-like velocities. Adapted from Kee et al. (2016).

While these sheets of material are geometrically thin, their high density and velocity combine to allow them to carry substantial amounts of material away from the disk. This is emphasised by Figure 5 (Kee et al. 2016, Figure 14), which shows the rate of change of mass in the simulation volume for disks around Be stars. Since the wind away from the disk is steady-state, this is the rate at which the disk loses mass by ablation. For all simulations we see that the disk ablation rate reaches a factor of an order of unity times the spherically symmetric wind mass loss rate. For later spectral types, this can be sustained due to the lower wind mass loss rate, while for the earliest spectral types considered it results in the disk being ejected dynamically from the simulation, shedding some light on the relative rareness of classical Oe stars in general and the tendency to find them in lower-metallicity environments where the stellar wind is weaker.

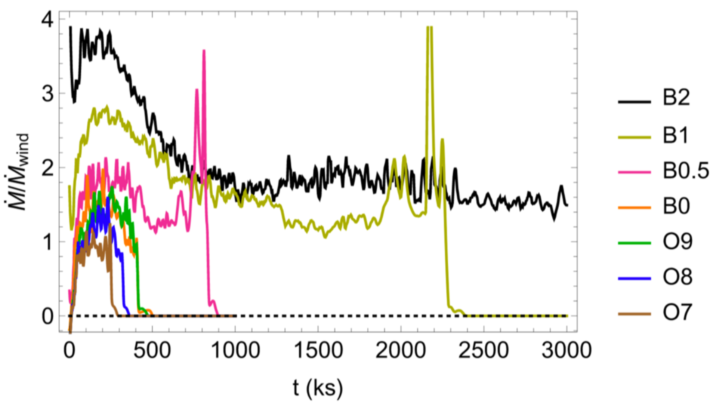

Fig. 5. Rate of disk destruction in the radiation-hydrodynamic simulations in units of the analytic, spherically-symmetric wind mass loss rate, $\dot{M}_{\rm wind}$. Adapted from Kee et al. (2016).

Looked at in a different way, we can instead quantify the time that the star will take to lose its disk. Motivated by the rates found in Figure 5, a good first order estimate should be the total mass of the disk divided by the wind mass loss rate. This is plotted in Fig. 6 (Kee et al. 2016, their Figure 15) with the actual disk destruction time from the simulations plotted for comparison. Given the generally good agreement between this estimate and the simulation results, we can take this one step further and compare it to photometric variability time-scales in observations of classical Be stars.

As an example, we can make a comparison with the recently published light-curve and model of ω CMa by Ghoreyshi et al. (2018). The model of the light-curve indicates that the disk loses $\sim 3\times10^{-9}M_\odot$ in each dissipation event, and from the stellar parameters provided the star has a mass loss rate $\sim 6\times10^{-10}M_\odot$ yr^{-1}. Taken together, this implies a disk ablation time of ~ 5 yr, well in line with the observed disk dissipation time for this star. From the modelling by Ghoreyshi et al. (2018), however, the observed light-curve is fitted well by

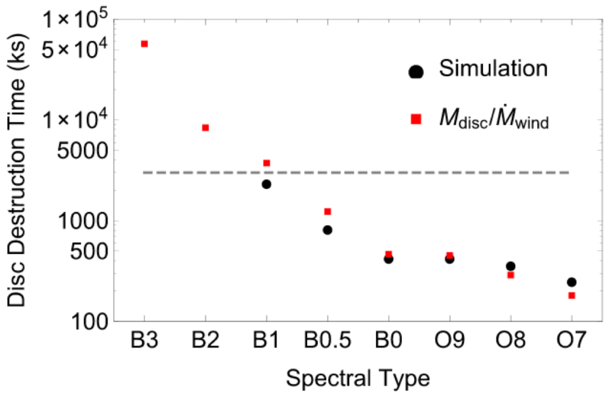

Fig. 6. Disk destruction time in the radiation-hydrodynamic simulations compared to a simple estimate given by the ratio of the disk mass, $M_{\rm disk}$, to the wind mass loss rate, $\dot{M}_{\rm wind}$. The grey dashed line shows the duration of the simulation. Adapted from Kee et al. (2016).

a viscous dissipation of the disk, highlighting the need for additional work to determine the interplay of these physical mechanisms in describing classical Be star disk destruction.

4 Conclusions

As emphasised by the two ongoing research areas discussed above, many efforts are currently under way to understand the structure of classical Be-star disks and the physical processes that govern them. The talk has also emphasised that these interpretations often require detailed, fully three-dimensional, radiation-hydrodynamics and radiation-transport models owing to the complex nature of the interplay between stellar irradiation and circumstellar disk material. Given the wealth of observational data that continues to flow in from observing missions like *BRITE*, however, the advancement of such models can proceed in step with the observational data to give us an ever improving view of the nature of these intriguing objects.

NDK would like to acknowledge funding from NASA ATP grant NNX11AC40G, under which a portion of the work presented here was completed, and the KU Leuven C1 grant MAESTRO for ongoing support.

References

Castor, J. I., Abbott, D. C., & Klein, R. I. 1975, ApJ, 195, 157
Ghoreyshi, M. R., Carciofi, A. C., Rímulo, L. R., et al. 2018, MNRAS, 479, 2214
Halonen, R. J. & Jones, C. E. 2013, ApJ, 765, 17
Kee, N. D., Owocki, S., & Sundqvist, J. O. 2016, MNRAS, 458, 2323
Marr, K. C., Jones, C. E., & Halonen, R. J. 2018, ApJ, 852, 103
Quirrenbach, A., Bjorkman, K. S., Bjorkman, J. E., et al. 1997, ApJ, 479, 477
Rivinius, T., Carciofi, A. C., & Martayan, C. 2013, A&A Rev., 21, 69